

High pressure studies of the T - P phase diagrams of erbium and thulium up to 30 GPa by using ac magnetization experiments

Masaki Mito¹* and Yuta Kimura*Graduate School of Engineering, Kyushu Institute of Technology, Kitakyushu 804-8550, Japan*Javier Campo²*Aragón Nanoscience and Materials Institute (CSIC - University of Zaragoza) and Physics Condensed Matter Department, C/Pedro Cerbuna 12, 50009 Zaragoza, Spain**and International Institute for Sustainability with Knotted and Chiral Meta Matter, 2-313 Kagamiyama, Higashi-Hiroshima City, Hiroshima, Japan 739-0046*

(Received 21 October 2023; revised 14 January 2024; accepted 24 January 2024; published 15 February 2024)

The pressure dependence of the magnetic ordering temperatures for lanthanide ferromagnets Er and Tm has been investigated in the pressure region of up to 30 GPa through ac magnetization measurements by employing a superconducting quantum interference device. Six $4f$ lanthanide ferromagnets, from Gd to Tm, commonly have successive structural transitions starting from a hexagonal close-packed (hcp) structure under pressure. The experiments reported here have been performed with high sensitivity to allow for a more comprehensive discussion of the magnetostructural correlation when compared to four other $4f$ ferromagnets, namely Gd, Tb, Dy, and Ho. Our results conclude that only Er exhibits the increase in ferromagnetic ordering temperature against initial compression among the six lanthanide ferromagnets. The ferromagnetic magnetization anomaly for Er reduces below the detection limit before the structural transformation from Sm-type to the dhcp structures, and that for Tm exhibits similar behavior before the structure transformation from the hcp to Sm-type structures. However, the helimagnetic magnetization anomalies of both Er and Tm remain stable at least within the Sm-type structure below 30 GPa.

DOI: [10.1103/PhysRevB.109.064414](https://doi.org/10.1103/PhysRevB.109.064414)

I. INTRODUCTION

The microscopic origin of the magnetization and the polarization variables is closely related with the degrees of freedom of the electron, charge, and spin, whereas their arrangement in a crystal lattice is related with the volume variable. Therefore, using stress it is possible to induce changes in the crystalline structures (volume variable), such as a change in the atomic distances or structural phase transitions, which modifies the electronic states near the Fermi surface, resulting in a change in the magnetic properties of metallic magnets. In this context, the connection between ferromagnetism and metallicity has been a crucial topic in solid state physics since long ago, which could be understood by first studying how the magnetic properties of ferromagnetic (FM) metals depend on the crystal structure. High-pressure experiments, capable of continuous structural manipulation over a wide range, have yielded valid physical information on this subject.

In fact, there exist only nine ferromagnetic metals constituted by a single atomic element: the three $3d$ transition metals (Fe, Co, and Ni) and the six $4f$ lanthanide metals (Gd, Tb, Dy, Ho, Er, and Tm). The ferromagnetism of $4f$ lanthanide ferromagnets is comprehended through the consideration of the Ruderman-Kittel-Kasuya-Yosida (RKKY) interaction among

the localized moments of the f -orbital electrons mediated by the conduction electrons [1–3]. The spatially damped oscillation of the spin polarization of conduction electrons could originate a competition between FM and antiferromagnetic (AFM) interactions, often leading to the formation of an incommensurate helimagnetic (HM) structure. Hereafter, the magnetic transition temperatures between the FM and HM states, as well as between the HM and paramagnetic (PM) states, are denoted by T_C and T_N , respectively. Regarding $4f$ lanthanide ferromagnets, Gd is irregular and only Gd has no T_N [4]. As the atomic number increases from Tb to Tm, both T_C and T_N decrease. Indeed, T_C barely changes within 20 ± 5 K for Ho, Er, and Tm [4].

All $4f$ lanthanide ferromagnets, from Gd to Tm, commonly have a hexagonal close-packed (hcp) structure at ambient pressure and undergo a structural transformation as the pressure increases according to the sequence; hcp \rightarrow rhombohedral Sm-type \rightarrow double-hcp (dhcp) \rightarrow face-centered cubic (fcc) \rightarrow trigonal structure, as shown in Fig. 1 [5–7]. For example, for the alkali metals Li, Na, K, Rb, and Cs, the body-centered cubic (bcc) structure with a filling factor of 68% changes to an fcc structure with a filling factor of 74%, leading to an hcp structure with the same filling factor of 74% [8]. The stacking of the hexagonal layers in fcc and hcp structures are ABC(A) and AB(A), respectively. In contrast, the $4f$ lanthanide ferromagnets display the opposite trend. They possess more complicated rhombohedral Sm-type

*mitoh@mns.kyutech.ac.jp

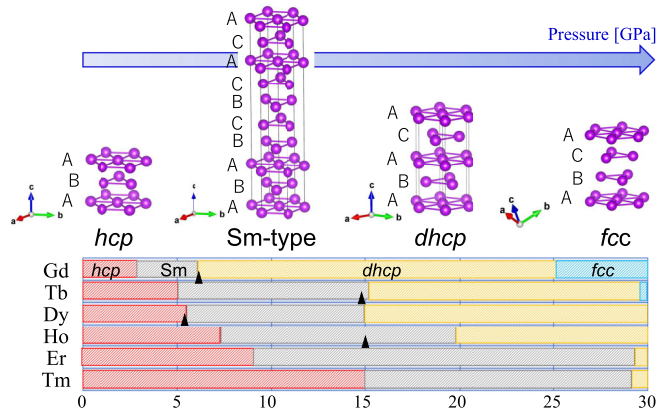


FIG. 1. Change in the crystal structure of $4f$ lanthanide ferromagnets under pressure [11]. The pressure region of each crystal structure refers to the experimental results at ambient temperature [7]. For reference, the black triangle in Gd–Ho represents the pressure above which the magnetic signal observed by the SQUID magnetometers becomes lower than the measurement noise level [11].

and dhcp structures between hcp and fcc structures as seen in Fig. 1. Moreover, there is a distinct difference in the stacking direction of hexagonal layers between dhcp and fcc structures. Indeed, Sm has an Sm-type structure at ambient pressure and exhibits complex properties [9], which change when the crystal structure is modified under pressure [10]. Thus, it is important to investigate the magnetic properties of the series of lanthanides Gd–Tm during the structural transformation from hcp \rightarrow Sm-type \rightarrow dhcp \rightarrow fcc.

The magnetic properties evolution with structural transformations for the six $4f$ FM metals were investigated by magnetic measurements (Gd–Ho [11–13], Gd [14], and Gd–Tm [15]), electrical resistance measurements (Gd [16–18], Tb [18–20], Dy [17,18,21], and Er [22,23]), neutron diffraction (Gd [24], Tb [19,25–27], Dy [28,29], and Ho [30,31]), Mössbauer spectroscopy (Dy [32]), and x-ray absorption near the edge structure (Dy [32]).

Magnetic measurements mainly are dominated by the magnetic moments of the localized $4f$ electrons, whereas resistivity measurements detect the transport properties of the conduction electrons correlated with the localized $4f$ electrons. Thus, resistivity measurements have been successfully conducted at pressures much higher than those employed in magnetic measurements because the accuracy of the measurements can be maintained with successful electrode construction.

However, we aimed to perform the magnetic measurements at high pressure. A detailed history of the magnetic measurements at high pressure is provided in Ref. [11]. Figure 1 illustrates an overview on the structural phase transition for Gd–Tm [5–7] and provides information on the critical pressure above which the magnetic signal for Gd–Ho cannot be detected in conventional magnetometry experiments: (i) ac magnetic susceptibility by the electromagnetic induction-type ac method using a high-frequency ac field (Gd–Ho [15]), (ii) both dc magnetization (Gd [14], Gd–Ho [13]) and (iii) ac magnetization using a commercial superconducting quantum interference device (SQUID) magnetometer and a miniature

DAC (Gd–Ho [11]), and (iv) dc magnetization by vibrating coil magnetometer methods using SQUID (Ho [11]).

Lanthanide ferromagnets Gd–Tm exhibits systematic structure transformation under pressure as mentioned above. Comprehensive understanding of the magnetostructural correlation in a series of six $4f$ FM metals Gd–Tm is very important to discuss the connection between ferromagnetism and metallicity. Given this background, the only available experimental data for Er and Tm are on ac magnetic susceptibility (Er [15], Tm [15]) and electrical resistivity (Er [22,23]), and there have been no reports on more reliable magnetization using a SQUID. Thus, in the present study, to comprehend the universal trend in the pressure effects on six $4f$ FM metals, the ac magnetization under pressure for Er and Tm has been measured using a SQUID magnetometer, which corresponds to the type (iii) measurement mentioned above.

II. METHODS

Polycrystalline samples of Er and Tm metals with a high purity (99.9%) were purchased from Nippon Yttrium Co., Ltd. In the high-pressure experiments some fragments with a volume of less than $0.1 \times 0.1 \times 0.1 \text{ mm}^3$ were employed.

A contraction corresponding to a stress of up to 30 GPa was achieved using an improved miniature CuBe DAC consisting of two diamond anvils with 0.5 mm diameter flat tips and a 0.25 mm thick Re gasket. The gasket was prepressed to apply pressure of above 20 GPa efficiently prior to inserting the sample into the sample chamber, so that the thickness was reduced down to below 0.15 mm. The original miniature DAC with the outer diameter of 8.5 mm was presented in Refs. [33,34]. In this experiment, diamond anvils of the Almax type with a culet of 0.5 mm were used. Apiezon-J oil (M&I Materials Limited), a liquidlike pressure-transmitting medium, was confined along with the small pieces of Er or Tm metal in the sample chamber. Because the space around the diamond anvils in the miniature DAC is too small to fill several pieces of metallic sample and a volatile pressure transmitting medium into the sample chamber, nonvolatile Apiezon-J oil with proper viscosity is suitable as the pressure transmitting medium to fill the sample chamber. The freezing point of the Apiezon-J oil at ambient pressure is 272 K. It is supposed that when we applied pressure of above 1 GPa at ambient temperature, the Apiezon-J oil would be solidified. The Apiezon-J oil with good thermal conductivity had often been used as pressure-transmitting medium in the heat capacity measurements [35,36] as well as magnetic measurements [36–38]. It was also used in the previous ac magnetization measurements for four lanthanide ferromagnets Gd–Ho [11]. The pressure at room temperature was evaluated by measuring the fluorescence of ruby [39] in the sample chamber.

The change in magnetization against the ac magnetic field was measured as the ac magnetization M_{ac} using a commercial SQUID magnetometer equipped with an ac source. Thus, the amplitude of H_{ac} was fixed at 3.9 Oe, and the frequency was selected to be low frequency as either 3 or 10 Hz. In the data analysis, the M_{ac} signal was divided into the in-phase m' and out-of-phase m'' components by Fourier transform. The m' at ambient pressure for polycrystalline Er and Tm was shown in Fig. 2, where there are the data for the frequency of 3 and

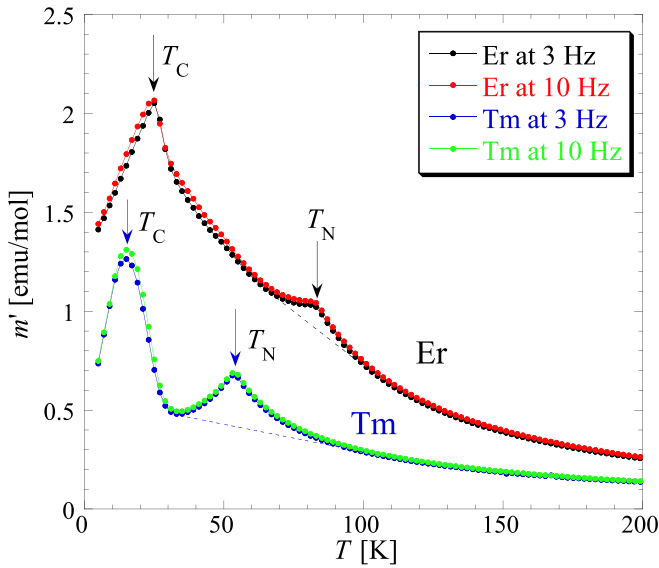


FIG. 2. T dependence of m' for Er (110.6 mg) and Tm (91.0 mg) polycrystalline samples. The ac magnetization was measured under an ac field with two frequency values of 3 and 10 Hz and an amplitude of 3.86 Oe using a commercial SQUID magnetometer. Two phase-transition temperatures, T_C and T_N , are marked with arrows. The broken lines help recognize the anomalies concerning T_N .

10 Hz. Between the results at two frequencies, there is quantitatively no meaningful difference. These accurate experiments enable to properly distinguish the two magnetic transitions from the background in a well-separated form. Most of the M_{ac} background signal in the pressure experiments using the miniature DAC originates from the eddy current of the CuBe metal, which is the main material of DAC. Therefore with increasing the frequency of H_{ac} , the intensity of background signal increases and broad humps appear over a wider temperature range. Indeed, most of the metallic background contributions appeared in m'' (out of phase for H_{ac}), while the magnetic signal of Er and Tm mainly appeared in m' (in phase for H_{ac}) [37,40–47]. Even if utilizing favorable phase separation, in the M_{ac} measurement using DAC, discerning between the two anomalies for Er and Tm is more challenging because of small T_N signal, compared to previous experiments involving Gd–Ho [11].

The temperature (T) dependence of the background signal can slightly change through high-pressure experiments, because the CuBe metal was partially compressed and a gasket was deformed. We could perform the background measurements prior to the measurement at the initial 0 GPa and after that at 0 GPa after applying maximum pressure, where the T dependence of background contribution at intermediate pressures rarely needs any calibration considering smooth change. In the next section, we will describe the background subtraction procedure for each experimental sequence.

III. EXPERIMENTAL RESULTS

A. Erbium

As seen in Fig. 2, the anomaly of T_C in Er has a wide cusp, whereas that of T_N is relatively narrow. Figure 3 shows the T

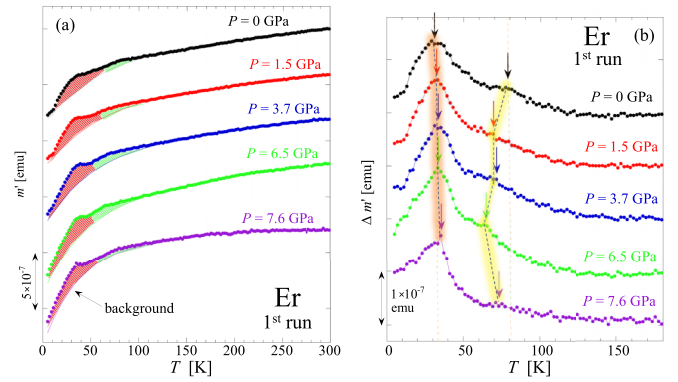


FIG. 3. T dependence of m' for Er under ac field with an amplitude of 3.86 Oe and a frequency of 10 Hz in the first run covering the P range up to 7.6 GPa (first run). The mass of Er sample, estimated from the signal intensity, is approximately 10 μ g. (a) m' including the background and (b) m' after subtracting the background contribution ($\Delta m'$). In (a), the background is shown with solid colored curve, and two types of magnetic anomalies are characterized by red and green areas. In (b), the beige and yellow lines with accompanying shadow arrows display the trend of change of the characteristic anomalies.

dependence of m' at different pressures in the range $0 \leq P \leq 7.6$ GPa for Er (first run). The m' - T data before background subtraction are shown in Fig. 3(a), and those obtained after background subtraction are depicted in Fig. 3(b). As seen in Fig. 3(a), at $P = 0$ GPa, there are two broad cusps at approximately 30 and 80 K, whose T dependences differ from that of the broader background signal. The T dependence of the background component varies slightly by pressurization because of gasket deformation by pressure. As seen in Fig. 3(b), background subtraction confirms the shapes of the two anomalies at 30 and 80 K, which are similar to the data in Fig. 2. As P increased, the low- T anomaly characterized by T_C shifted slightly toward the higher T , whereas the high- T anomaly characterized by T_N shifted slightly toward the lower T . At $P = 6.5$ GPa, T_N was estimated to be ~ 65 K. At $P = 7.6$ GPa, close to the P value of the structural transition from hcp to the Sm-type structures, the detection of the T_N anomaly becomes difficult, and a careful observation of the corresponding area enabled T_N to be estimated at approximately 56 K. Moreover, for $P = 7.6$ GPa, there was also a broad anomaly at ~ 80 K.

Figure 4 shows the T dependence of m' up to $P = 29.5$ GPa (second run) for Er. The result at $P = 0$ in the second run was consistent with that of the first run. As seen in Fig. 4(b), at $P = 11.6$ GPa, which is higher than the maximum P in the first run, T_C increases to ~ 35 K, and there is another anomaly at ~ 75 K. These results were qualitatively consistent with those at the maximum pressure, $P = 7.6$ GPa, in the first run. At further pressurization, $P = 16.4$ GPa, a broad anomaly presented with hatching was observed, which appeared to be composed of two anomalies at 35 and 43 K at $P = 11.6$ GPa. At $P = 23.4$ and 29.5 GPa, the magnetic signal on the low- T region was reduced below the measurement noise level, and only one anomaly was observed near 70 K. The discrete change in the T_N anomaly observed for Er was phenomenologically similar to that observed for Tb [11]. The convergence of

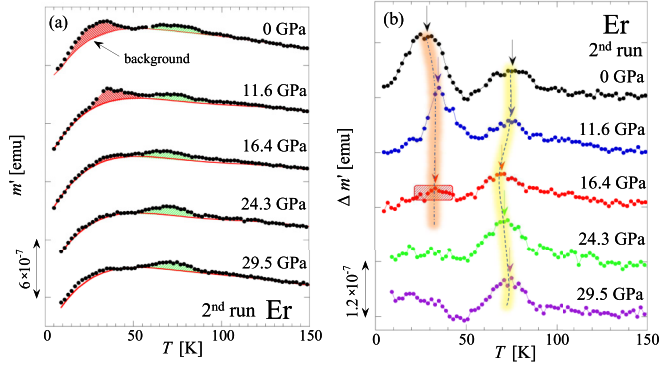


FIG. 4. T dependence of m' under ac field of 10 Hz for Er of the second run covering the P range up to 29.5 GPa (second run). The mass of Er sample, estimated from the signal intensity, is approximately 11 μg . (a) m' including the background and (b) m' after subtracting the background contribution ($\Delta m'$). In (a), the background is shown with a red curve, and the two types of magnetic anomalies are characterized by red and green areas. In (b), the beige and yellow lines with accompanying shadow arrows display the trend of change in the characteristic anomalies. The trend from 0 to 11.6 GPa is referred to in Fig. 3.

the T_C anomaly and the low- T side of the split T_N anomalies exhibited similarities to what has been observed in Ho [11] and later Tm.

Figure 5 shows the P dependence of the characteristic temperatures T_N and T_C for Er. The disappearance of the FM magnetization anomaly, characterized as T_C , was also observed for Gd, Tb, Dy, and Ho [11], whereas the stability of ferromagnetism for Er was higher than that for Gd–Ho. In contrast, the survival of the HM magnetization anomaly near its initial T_N was also observed for Tb [11]. The other overall behaviors are consistent with previous results in the

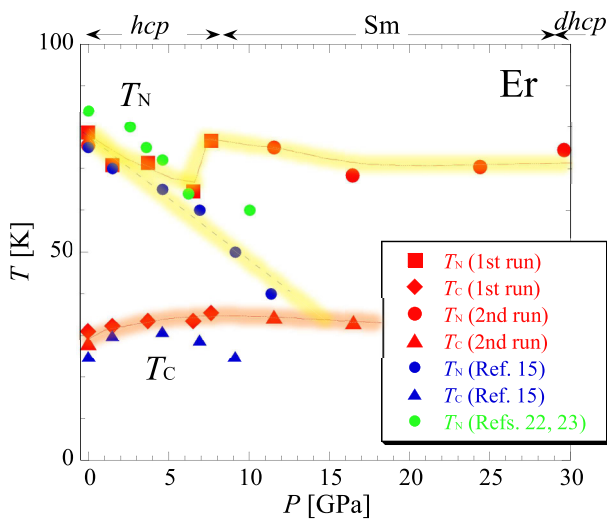


FIG. 5. Pressure dependence of T_N and T_C along with the results of previous studies by Thomas *et al.* [22,23] (R) and Jackson *et al.* [15] (χ). The beige and yellow lines with accompanying shadow arrows display the trend of change in the characteristic anomalies. The discrete change in T_N has already been observed for Tb [11].

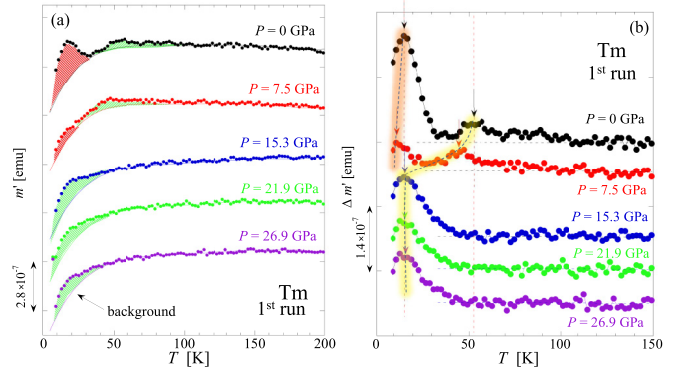


FIG. 6. T dependence of m' under ac field of 3 Hz for Tm (first run). (a) m' along with the background and (b) m' after subtracting the background contribution ($\Delta m'$). The mass of Tm sample, estimated from the signal intensity, is approximately 30 μg . In (a), the background is shown with a colored curve, and two types of magnetic anomalies are characterized by red and green areas. In (b), the beige and yellow lines with accompanying shadow arrows display the trend of change in characteristic anomalies. The temperature position for T_N at $P = 0$ GPa is presented by a red dotted line, and the baseline of the vertical axis at each pressure is presented by a black dotted line.

literature (magnetic susceptibility [15], resistivity [22,23]), except for the possibility that the high- T anomaly of the split T_N anomalies remained in the considered P range. Indeed, we could not conclude the splitting of T_N anomalies because of insufficient accuracy. However, if a small cusp at 43 K, not characterized as T_C , at $P = 11.6$ GPa would be real, it could be plotted on the line representing the trend of T_N in Ref. [15].

B. Thulium

As seen in Fig. 2, both anomalies concerning T_C and T_N for Tm are well separated, with prominent valleys being the former, sharper than the latter. For Tm, the T dependence of m' under pressure was measured along three runs. Figure 6 shows the T dependence of m' for Tm in the first run for $P \leq 26.9$ GPa. The m' - T data before and after background subtraction are shown in Figs. 6(a) and 6(b), respectively. As seen in Fig. 6(a), at $P = 0$ GPa, there are two broad peaks at approximately 15 and 50 K. At $P = 7.5$ GPa, both anomalies shift toward lower T , keeping almost the same difference of 30–35 K. This behavior was confirmed in the data after background subtraction, as shown in Fig. 6(b). Upon further pressurization to $P = 15.3$, 21.9, and 26.9 GPa, only one anomaly remained at ~ 15 K. This phenomenon was also observed at $P = 28.6$ GPa in the second run, as shown in Fig. 7. By omitting the measurements near 10–20 GPa, the pressure near 30 GPa can be achieved with high possibility. The results of the first and second runs suggest that the T_C anomaly might remain at ~ 15 K and the T_N anomaly would disappear near $P = 10$ GPa. However, this assumption was rejected in the third run of the experiments.

Figure 8 shows the T dependence of m' in the third run, where the P region compensates for the region between 7.5 and 15.3 GPa in the first run. Figures 8(a) and 8(b) show the data before and after background subtraction, respectively. The figures show that the T_N anomaly shifted toward the lower

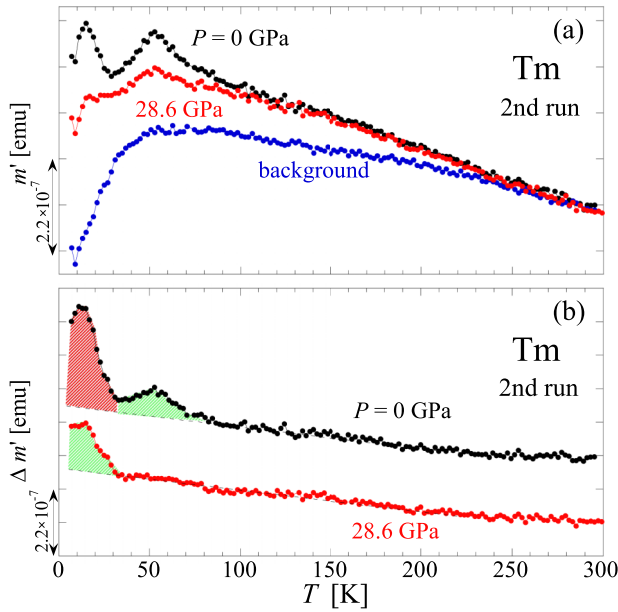


FIG. 7. T dependence of m' and $\Delta m'$ under ac field of 3 Hz for Tm (second run). Two types of magnetic anomalies are characterized by red and green areas. The mass of Tm sample, estimated from the signal intensity, is approximately 40 μg . In (b), the baseline of the vertical axis at each pressure is presented by a black dotted line.

T , increasing the magnitude of m' . This result indicates that the T_C anomaly disappeared at $P = 10.0$ GPa, whereas the T_N anomaly at $P = 14.2$ GPa remained at a temperature of ~ 15 K.

Figure 9 shows the P dependence of the characteristic temperatures, such as T_N and T_C for Tm, and the series of data is consistent with previous results in the literature (magnetic susceptibility [15]). If the measurements were restricted to below 20 K, we would recognize that T_C for Tm

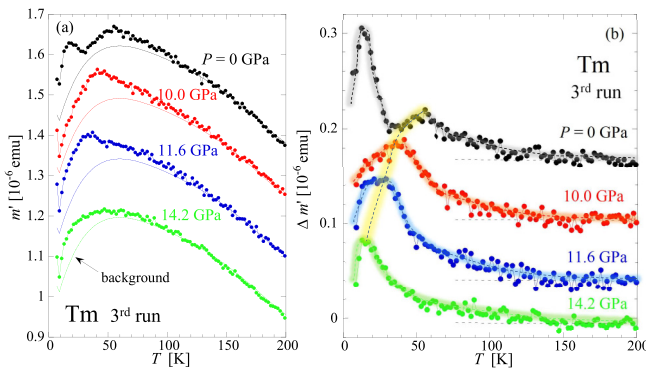


FIG. 8. T dependence of m' under ac field of 3 Hz for Tm (third run). (a) m' along with the background and (b) m' after subtracting the background contribution ($\Delta m'$). The mass of the Tm sample, estimated from the signal intensity, is approximately 18 μg . In (a), the background is shown solid colored, and the two types of magnetic anomalies are characterized by red and green areas. In (b), the baseline of the vertical axis at each pressure is presented by a black dotted line. In (a) and (b), the trend of change in the characteristic anomaly concerning T_N is displayed by a yellow line with a shadow.

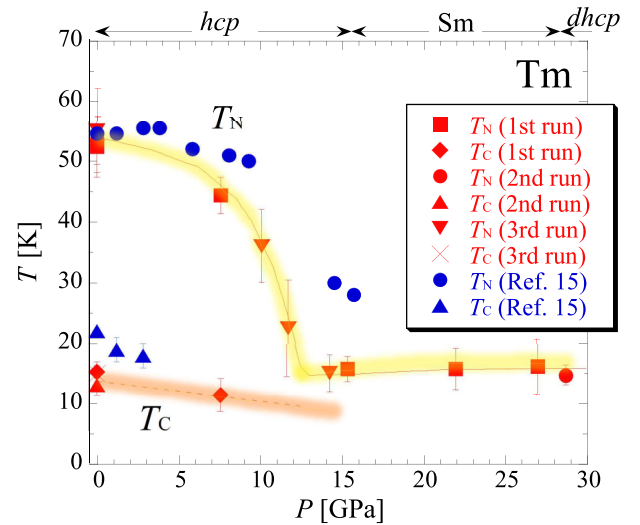


FIG. 9. T_N and T_C along with the results of a previous study by Jackson *et al.* [15]. The beige and yellow lines with accompanying shadow arrows display the trend of change in the characteristic anomalies. The obtained pressure response is similar to that for Ho [11].

hardly changes under pressure. However, the measurement for the temperatures down to 5 K revealed that the FM magnetization anomaly for Tm disappears, shifting toward the low temperature side, contrary to the disappearance of the FM magnetization anomaly shifting toward the high temperature side for Er. According to recent neutron diffraction studies of Ho at $P = 8$ GPa, the FM order disappears and the HM order remains until low temperatures [31]. This instability of the FM order under pressure is a common feature for the FM lanthanides, including Gd, Tb, Dy, Ho, Er, and Tm [11]. The survival of the HM magnetization anomaly for Tm was also observed, similarly to Er. However, the P dependence of T_N , as observed, exhibited similarities to that of Ho with the transformation from the FM order into the HM order at low temperatures, as reported in a recent study [31].

IV. DISCUSSION

The magnetic structure of Tm was investigated approximately 60 years ago. It was reported that the magnetic ordered state below T_C was ferrimagnetic based on a magnetic unit cell of the up-up-down-down structure [48]. Here we deduce that the FM ordering of Tm has been shown to be unstable under pressure, as depicted in Fig. 9. On the contrary, it is noted that only T_C for Er exhibits the increase against initial compression among the six lanthanide ferromagnets Gd–Tm and it survives in the P region up to 17 GPa.

Figure 10 shows an overview of the stability of both the HM and FM orders in the lanthanide FM metals Gd, Tb, Dy, Ho, Er, and Tm from the viewpoint of magnetostructural correlation. Here, the measurement limit of magnetization has been determined by the measurement accuracy of the SQUID magnetometer. The Gd–Ho results using the SQUID magnetometer have been published elsewhere [11]. Generally, for all six elements, the FM magnetization anomaly finally

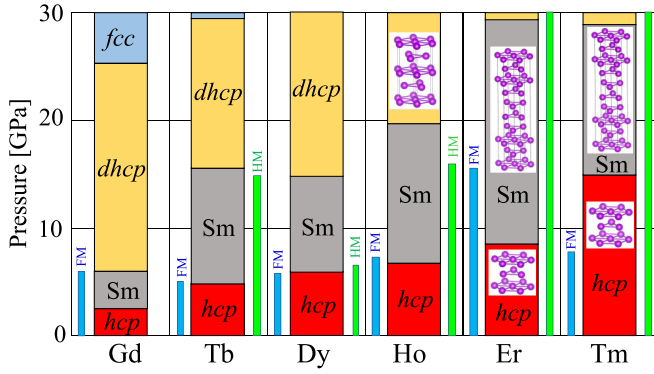


FIG. 10. Magnetostructural correlation of a series of lanthanide FM metals at pressures up to 30 GPa. The results for Gd–Ho have already been reported [11]. Herein, the results of Er and Tm are included. The light blue and green bars represent the P region, in which the FM and HM signals observed by the SQUID magnetometers become higher than the measurement noise.

disappears at high pressures; (i) FM magnetization anomaly in Tb, Dy, and Ho becomes unstable at a critical pressure at which the transition from hcp to Sm-type structures occurs; (ii) the FM magnetization anomaly in Gd and Er remains for the Sm-type structure and disappears near or before the structural transformation to the dhcp structure; and (iii) the FM magnetization anomaly of Tm is the most unstable among

the six elements and disappears below the boundary between the hcp and the Sm-type structures.

Regarding the HM magnetization anomaly, the disappearance of the corresponding magnetic signal for Tb and Ho are observed along with the structural transformation from the Sm-type to the dhcp structure. The HM order of Er and Tm appears to be more stable than that of Tb and Ho. The HM order of Dy is the most unstable and the corresponding magnetization anomaly disappears along with the FM order. Generally, as the number of $4f$ electrons increases, the stability of the HM order against contraction tends to increase.

As mentioned above, the pressure dependences of T_C and T_N for the six $4f$ lanthanide ferromagnets Gd–Tm do not show a consistent behavior, and strictly depend on the element. However, careful observation of the common trend allows the categorization of the P dependence of T_C and T_N into three categories as shown in Fig. 11: (i) Gd and Dy, (ii) Tb and Er, and (iii) Ho and Tm. In the first category (i) for Gd and Dy, both T_C and T_N exhibit a linear decrease as a function of pressure. Beyond the critical pressure related to the structural transition, the magnetic anomalies at T_C and T_N disappear. The second category (ii) for Tb and Er shows that T_N undergoes a discretelike change associated with structural transformation. Subsequently, the T_N anomaly persists near the initial T region even after the T_C anomaly has disappeared. In the third category (iii) for Ho and Tm, T_N approaches T_C , and T_N remains close to the initial T_C value after the disappearance of the T_C anomaly.

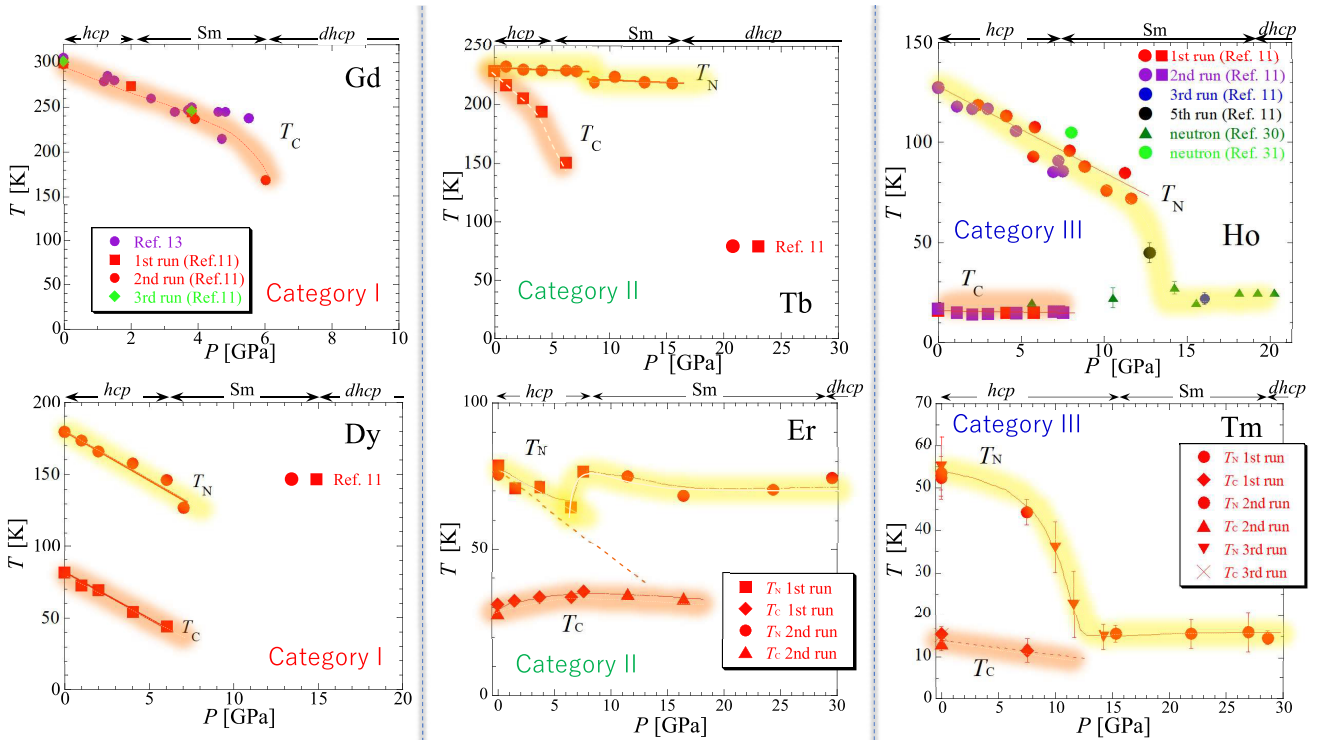


FIG. 11. Categorized figure of the P dependence of T_C and T_N , determined by the SQUID magnetometers, for six lanthanide FM metals. The results for Gd, Tb, Dy, and Ho are shown in Refs. [11,31]. The results of T_N for Ho at 12.7 and 16.0 GPa were reconsidered as meaningful data in the present study [11]. For Ho, the results by neutron diffraction are also plotted as the reference data [30,31]. Beige and yellow curves with shadows express the trends of T_C and T_N , respectively. The P dependences of T_C and T_N are categorized into three categories, namely (i) Gd and Dy, (ii) Tb and Er, and (iii) Ho and Tm.

Indeed, in order to investigate the magnetic structure and conclude whether the FM and HM order survive or not under pressure, the neutron diffraction experiments with high accuracy are required. There have already been many pioneering reports of neutron diffraction in Gd [24], Tb [19,25–27], Dy [28,29], and Ho [30,31]. In the future, as more careful experiments, the neutron diffraction experiments for a wider d -spacing region and using a higher energy source under better hydrostatic-pressure conditions are desirable. Indeed, the high-pressure XRD analyses at low temperatures are also necessary to conduct reliable analyses of magnetic structures. Finally, the results of magnetization measurement, low-temperature XRD analyses, and neutron diffraction are needed to be discussed along with the results of electrical resistance measurements (Gd [16–18], Tb [18–20], Dy [17,18,21], and Er [22,23]).

The density of state near the Fermi energy level is the crucial factor to determine the magnetic interaction of metallic ferromagnets [49]. Thus, to discuss the aforementioned phenomena in detail, it is imperative to perform electronic state determinations using first-principles calculations under pressure and the subsequent calculations of the RKKY interaction. In addition, electronic state calculations when considering the spin contribution are required, and these are challenging tasks. Finally, let us mention the present status for Gd. Experimentally, for Gd, the FM magnetization anomaly remains in the hcp and Sm-type structure, whereas the intensity of magnetization decreases after the structural phase transformation from hcp and Sm-type structure [11,13,14]. Recently, for Gd, the pioneering study of DFT has been reported, and it is

suggested that the Sm-type and dhcp structures favor the AFM interaction consistently with the experimental results [50].

V. CONCLUSION

To conclude, the Sm-type structure stabilized under pressure in both Er and Tm did not favor the FM order, whereas it allowed the existence of the T_N anomaly. In both Er and Tm, the HM order survives in the pressure region up to 30 GPa. The FM state of Er is the most stable from among Gd–Tm, and only Er exhibits the increase in T_C in the P region up to approximately 17 GPa. For $P > 20$ GPa, T_C cannot be determined experimentally for all metals mentioned herein. The pressure dependences of T_C and T_N for the six lanthanide ferromagnets were categorized into three divisions: (i) Gd and Dy, (ii) Tb and Er, and (iii) Ho and Tm. In future work, electronic state calculations using first-principles calculations along with the high-pressure XRD analyses at low temperatures are necessary to elucidate the common features of each category.

ACKNOWLEDGMENTS

This work was supported by JSPS KAKENHI Grants No. 23H01126, No. 21K18606, No. 19KK0070, and No. 17H03379. J.C. acknowledges support by Grants No. PID2022-138492NB-I00-XM4 funded by MCIN/AEI/10.13039.501100011033, No. OTR02223-SpINS from CSIC/MCIN, and No. DGA/M4 from Diputación General de Aragón (Spain).

-
- [1] M. A. Ruderman and C. Kittel, Indirect exchange coupling of nuclear magnetic moments by conduction electrons, *Phys. Rev.* **96**, 99 (1954).
- [2] T. Kasuya, A theory of metallic ferro- and antiferromagnetism on Zener's model, *Prog. Theor. Phys.* **16**, 45 (1956).
- [3] K. Yosida, Magnetic properties of Cu-Mn alloys, *Phys. Rev.* **106**, 893 (1957).
- [4] S. Chikazumi, *Physics of Ferromagnetism* (Oxford University Press, New York, 1997).
- [5] J. Akella, G. S. Smith, and A. P. Jephcoat, High-pressure phase transformation studies in gadolinium to 106 GPa, *J. Phys. Chem. Solids* **49**, 573 (1988).
- [6] W. A. Grosshans and W. B. Holzapfel, Atomic volumes of rare-earth metals under pressures to 40 GPa and above, *Phys. Rev. B* **45**, 5171 (1992).
- [7] G. K. Samudrala and Y. K. Vohra, Structural properties of lanthanides at ultra high pressure, in *Handbook on the Physics and Chemistry of Rare Earths* (Elsevier, North-Holland, 2013), Vol. 43, pp. 275–319.
- [8] V. F. Degtyareva, Potassium under pressure: Electronic origin of complex structures, *Solid State Sci.* **36**, 62 (2014).
- [9] W. C. Koehler and R. M. Moon, Magnetic structures of samarium, *Phys. Rev. Lett.* **29**, 1468 (1972).
- [10] M. Mito, H. Kondo, T. Arase, K. Irie, S. Takagi, H. Deguchi, T. Tajiri, and M. Ishizuka, High-pressure magnetic properties of antiferromagnetic samarium up to 30 GPa using a SQUID-based vibrating coil magnetometer, *Phys. Rev. B* **104**, 054431 (2021).
- [11] M. Mito, Y. Kimura, K. Yamakata, M. Ohkuma, H. Chayamichi, T. Tajiri, H. Deguchi, and M. Ishizuka, Relationship of magnetic ordering and crystal structure in lanthanide ferromagnets Gd, Tb, Dy, and Ho at high pressures, *Phys. Rev. B* **103**, 024444 (2021).
- [12] D. B. McWhan and A. L. Stevens, Effect of pressure on the magnetic properties and crystal structure of Gd, Tb, Dy, and Ho, *Phys. Rev.* **139**, A682 (1965).
- [13] M. Mito, K. Matsumoto, Y. Komorida, H. Deguchi, S. Takagi, T. Tajiri, T. Iwamoto, T. Kawae, M. Tokita, and K. Takeda, Volume shrinkage dependence of ferromagnetic moment in lanthanide ferromagnets gadolinium, terbium, dysprosium, and holmium, *J. Phys. Chem. Solids* **70**, 1290 (2009).
- [14] T. Iwamoto, M. Mito, M. Hitaka, T. Kawae, and K. Takeda, Magnetic measurement of rare earth ferromagnet gadolinium under high pressure, *Phys. B: Condens. Matter* **329-333**, 667 (2003).
- [15] D. D. Jackson, V. Malba, S. T. Weir, P. A. Baker, and Y. K. Vohra, High-pressure magnetic susceptibility experiments on the heavy lanthanides Gd, Tb, Dy, Ho, Er, and Tm, *Phys. Rev. B* **71**, 184416 (2005).
- [16] G. K. Samudrala, G. M. Tsoi, S. T. Weir, and Y. K. Vohra, Structural and magnetic phase transitions in gadolinium under

- high pressures and low temperatures, *High Pressure Res.* **34**, 385 (2014).
- [17] J. Lim, G. Fabbri, D. Haskel, and J. S. Schilling, Magnetic ordering at anomalously high temperatures in Dy at extreme pressure, *Phys. Rev. B* **91**, 045116 (2015).
- [18] J. Lim, G. Fabbri, D. Haskel, and J. S. Schilling, Record high magnetic ordering temperature in a lanthanide at extreme pressure, *J. Phys.: Conf. Ser.* **950**, 042025 (2017).
- [19] S. A. Thomas, J. M. Montgomery, G. M. Tsoi, Y. K. Vohra, G. N. Chesnut, S. T. Weir, C. A. Tulk, and A. M. dos Santos, Neutron diffraction and electrical transport studies on magnetic ordering in terbium at high pressures and low temperatures, *High Pressure Res.* **33**, 555 (2013).
- [20] J. Lim, G. Fabbri, D. Haskel, and J. S. Schilling, Anomalous pressure dependence of magnetic ordering temperature in Tb revealed by resistivity measurements to 141 GPa: Comparison with Gd and Dy, *Phys. Rev. B* **91**, 174428 (2015).
- [21] G. K. Samudrala, G. M. Tsoi, S. T. Weir, and Y. K. Vohra, Magnetic ordering temperatures in rare earth metal dysprosium under ultrahigh pressures, *High Pressure Res.* **34**, 266 (2014).
- [22] S. A. Thomas, G. M. Tsoi, L. E. Wenger, Y. K. Vohra, and S. T. Weir, Magnetic and structural phase transitions in erbium at low temperatures and high pressures, *Phys. Rev. B* **84**, 144415 (2011).
- [23] S. A. Thomas, G. M. Tsoi, L. E. Wenger, Y. K. Vohra, and S. T. Weir, Magnetic transitions in erbium at high pressures, *J. Appl. Phys.* **111**, 07E104 (2012).
- [24] N. O. Golosova, D. P. Kozlenko, E. V. Lukin, S. E. Kichanov, and B. N. Savenko, High pressure effects on the crystal and magnetic structure of ^{160}Gd metal, *J. Magn. Magn. Mater.* **540**, 168485 (2021).
- [25] H. Umebayashi, G. Shirane, B. C. Frazer, and W. B. Daniels, Neutron diffraction study of Tb and Ho under high pressure, *Phys. Rev.* **165**, 688 (1968).
- [26] S. Kawano, N. Achiwa, A. Onodera, and Y. Nakai, Neutron diffraction studies of pressure effects on magnetic structures of Tb, *Phys. B: Condens. Matter* **180&181**, 46 (1992).
- [27] M. P. Clay, R. Sereika, W. Bi, and Y. K. Vohra, Magnetic ordering in terbium at high pressures and low temperatures, *J. Magn. Magn. Mater.* **580**, 170935 (2023).
- [28] C. Perreault, Y. K. Vohra, A. M. dos Santos, J. J. Molaison, and R. Boehler, Magnetic ordering in rare earth metal dysprosium revealed by neutron diffraction studies in a large-volume diamond anvil cell, *High Pressure Res.* **39**, 588 (2019).
- [29] C. S. Perreault, Y. K. Vohra, A. M. dos Santos, and J. J. Molaison, Magnetic structure of antiferromagnetic high-pressure phases of dysprosium, *J. Magn. Magn. Mater.* **545**, 168749 (2022).
- [30] C. S. Perreault, Y. K. Vohra, A. M. dos Santos, and J. J. Molaison, Neutron diffraction study of magnetic ordering in high pressure phases of rare earth metal holmium, *J. Magn. Magn. Mater.* **507**, 166843 (2020).
- [31] M. Pardo-Sainz, F. Cova, J. A. Rodríguez-Velamazán, I. Puente-Orench, Y. Kousaka, M. Mito, and J. Campo, Revisiting the magnetic structure of Holmium at high pressure by using neutron diffraction, *Sci. Rep.* **13**, 12168 (2023).
- [32] W. Bi, E. Alp, J. Song, Y. Deng, J. Zhao, M. Hu, D. Haskel, and J. M. Schilling, Studies of magnetism in dysprosium under extreme pressures, *MAR17 Meeting of APS*, <https://meetings.aps.org/Meeting/MAR17/Session/B35.15>, 2017.
- [33] M. Mito, M. Hitaka, T. Kawae, K. Takeda, T. Kitai, and N. Toyoshima, Development of miniature diamond anvil cell for the superconducting quantum interference device magnetometer, *Jpn. J. Appl. Phys.* **40**, 6641 (2001).
- [34] M. Mito, Magnetic measurements on molecule-based magnets under high pressure, *J. Phys. Soc. Jpn. Suppl. A* **76**, 182 (2007).
- [35] K. Takeda, M. Wada, M. Inoue, and T. Haseda, Measurement of heat capacity under hydrostatic pressure between 0.5 K and 15 K, *Jpn. J. Appl. Phys.* **26**, 947 (1987).
- [36] M. Mito, H. Deguchi, T. Tanimoto, T. Kawae, S. Nakatsuji, H. Morimoto, H. Anzai, H. Nakao, Y. Murakami, and K. Takeda, Pressure effects on an organic radical ferromagnet: 2,5-difluorophenyl- α -nitronyl nitroxide, *Phys. Rev. B* **67**, 024427 (2003).
- [37] M. Mito, K. Ogata, H. Goto, K. Tsuruta, K. Nakamura, H. Deguchi, T. Horide, K. Matsumoto, T. Tajiri, H. Hara *et al.*, Uniaxial strain effects on the superconducting transition in Re-doped Hg-1223 cuprate superconductors, *Phys. Rev. B* **95**, 064503 (2017).
- [38] K. Irie, K. Shibayama, M. Mito, S. Takagi, M. Ishizuka, K. Lakin, and R. T. Oakley, High-pressure dc magnetic measurements on a bisdiselenazolyl radical ferromagnet using a vibrating-coil SQUID magnetometer, *Phys. Rev. B* **99**, 014417 (2019).
- [39] G. J. Piermarini, S. Block, J. D. Barnett, and R. A. Forman, Calibration of the pressure dependence of the R_1 ruby fluorescence line to 195 kbar, *J. Appl. Phys.* **46**, 2774 (1975).
- [40] M. Mito, Y. Komorida, H. Tsuruda, J. S. Tse, S. Desgreniers, Y. Ohishi, A. A. Leitch, K. Cvrkalj, C. M. Robertson, and R. T. Oakley, Heavy atom ferromagnets under pressure: Structural changes and the magnetic response, *J. Am. Chem. Soc.* **131**, 16012 (2009).
- [41] A. A. Leitch, K. Lakin, S. M. Winter, L. E. Downie, H. Tsuruda, J. S. Tse, M. Mito, S. Desgreniers, P. A. Dube, S. Zhang *et al.*, From magnets to metals: The response of tetragonal bisdiselenazolyl radicals to pressure, *J. Am. Chem. Soc.* **133**, 6051 (2011).
- [42] H. Tsuruda, M. Mito, H. Deguchi, S. Takagi, A. A. Leitch, K. Lakin, S. M. Winter, and R. T. Oakley, Pressure dependence of curie temperature in a selenazolyl radical ferromagnet, *Polyhedron* **30**, 2997 (2011).
- [43] S. Yamaguchi, N. Yamaguchi, M. Mito, H. Deguchi, P. J. Baker, S. J. Blundell, M. J. Pitcher, D. R. Parker, and S. J. Clarke, AC magnetic measurement of LiFeAs at pressures up to 5.2 GPa: The relation between T_c and the structural parameter, *J. Korean Phys. Soc.* **63**, 445 (2013).
- [44] M. Mito, T. Imakyurei, H. Deguchi, K. Matsumoto, H. Hara, T. Ozaki, H. Takeya, and Y. Takano, Effective disappearance of the meissner signal in the cuprate superconductor $\text{YBa}_2\text{Cu}_4\text{O}_8$ under uniaxial strain, *J. Phys. Soc. Jpn.* **83**, 023705 (2014).
- [45] M. Mito, H. Goto, H. Matsui, H. Deguchi, K. Matsumoto, H. Hara, T. Ozaki, H. Takeya, and Y. Takano, Uniaxial strain effects on superconducting transition in $\text{Y}_{0.98}\text{Ca}_{0.02}\text{Ba}_2\text{Cu}_4\text{O}_8$, *J. Phys. Soc. Jpn.* **85**, 024711 (2016).
- [46] M. Mito, Y. Kitamura, T. Tajiri, K. Nakamura, R. Shiraishi, K. Ogata, H. Deguchi, T. Yamaguchi, N. Takeshita, T. Nishizaki *et al.*, Hydrostatic pressure effects on superconducting transition of nanostructured niobium highly strained by high-pressure torsion, *J. Appl. Phys.* **125**, 125901 (2019).

- [47] M. Mito, S. Shigeoka, H. Kondo, N. Noumi, Y. Kitamura, K. Irie, K. Nakamura, S. Takagi, H. Deguchi, T. Tajir *et al.*, Hydrostatic compression effects on fifth-group element superconductors V, Nb, and Ta subjected to high-pressure torsion, *Mater. Trans.* **60**, 1472 (2019).
- [48] W. C. Koehler, J. W. Cable, E. O. Wollan, and M. K. Wilkinson, Magnetic structures of thulium, *Phys. Rev.* **126**, 1672 (1962).
- [49] M. Tokita, K. Zenmyo, H. Kubo, K. Takeda, M. Mito, and T. Iwamoto, RKKY interaction in metallic Gd in GPa pressure regions, *J. Magn. Magn. Mater.* **272-276**, 593 (2004).
- [50] R. M. Vieira, O. Eriksson, T. Bjökman, O. Šipr, and H. C. Herper, The role of pressure-induced stacking faults on the magnetic properties of gadolinium, [arXiv:2309.01285](https://arxiv.org/abs/2309.01285).